American Mineralogist, Volume 94, pages 352–358, 2009

High-pressure structural behavior of ingersonite, $Ca_3Mn^{2+}Sb_4^{5+}O_{14}$: An in-situ single-crystal X-ray study

Pier Francesco Zanazzi,[1,*] Laura Chelazzi,[2] Paola Bonazzi,[2] and Luca Bindi[3]

[1]Dipartimento di Scienze della Terra, Università di Perugia, Piazza dell'Università, I-06100 Perugia, Italy
[2]Dipartimento di Scienze della Terra, Università di Firenze, via La Pira 4, I-50121 Firenze, Italy
[3]Museo di Storia Naturale, sezione di Mineralogia, Università di Firenze, via La Pira 4, I-50121 Firenze, Italy

Abstract

An in-situ, high-pressure, single-crystal X-ray diffraction study has been carried out at room temperature up to 7.42 GPa on a crystal of ingersonite, ideally $Ca_3Mn^{2+}Sb_4^{5+}O_{14}$, from the type material. Ingersonite is isostructural with the synthetic weberite-3*T* polytype and related to the pyrochlore structure-type. Owing to the *P* range investigated and the quality of data, a second-order Birch-Murnaghan Equation of State (EoS) is the best approximation to describe the ingersonite volume evolution with *P*. The refined EoS parameters are V_0 = 810.6(1) Å^3 and K_0 = 154.5(2.4) GPa. The behavior of ingersonite with pressure is almost isotropic and the decrease of the unit-cell volume is mainly due to the kinking of the polyhedra rather than their volume decrease. The overall mean distances are quite constant, indicating virtually no compressibility of both the A and B polyhedra in the *P* range investigated. However, some geometrical changes in the pyrochlore-like AB_3 layer can be observed and compared with those observed in synthetic pyrochlore compounds. The largest change is observed for the *z* atomic coordinate of the O2 atom. Using an anion-centered polyhedral description, O2 is the only O atom that is asymmetrically located in an octahedral interstice, this feature being the most remarkable difference between the structure of ingersonite (i.e., weberite-3*T* type, space group $P3_121$) and that of zirconolite-3*T* (pyrochlore structure type, space group $P3_121$), where all the O atoms occupy the tetrahedral interstices of a cubic A_2B_2 array. With the increase of pressure, the O2 atom migrates from the A_4B_2 octahedral cavity toward the adjacent AB_3 tetrahedral cavity, suggesting that a transition from weberite-3*T* to zirconolite-3*T* structure type could occur at pressures higher than 11 GPa.

Keywords: Ingersonite, high pressure, compressibility, crystal structure, phase transition

Introduction

Several different polytypes are known among synthetic weberite-type fluorides and oxides having an ideal stoichiometry $A_2B_2X_7$, including 2*M*, 4*M,* 3*T* (Yakubovich et al. 1994), and 6*T* (Grey and Roth 2000). In this view, the mineral weberite itself, Na_2MgAlF_7, which shows orthorhombic symmetry (Giuseppetti and Tadini 1978), is the 2*O* polytype. Recently, it was shown that ingersonite, $Ca_3Mn^{2+}Sb_4^{5+}O_{14}$, is isostructural with the weberite-3*T* polytype (Bonazzi and Bindi 2007). To our knowledge, the only natural members belonging to the weberite-type polytypic series are weberite and ingersonite. In contrast, most of the minerals having the ideal stoichiometry $A_2B_2X_7$ (A = Ca^{2+}, Na^+, K^+, Sr^{2+}, Ba^{2+}, Sn^{2+}, Pb^{2+}, REE^{3+}, Y^{3+}, Sb^{3+}, Bi^{3+}, U^{4+}; B = Nb^{5+}, Ta^{5+}, Ti^{4+}, Sb^{5+}, Fe^{3+}, Sn^{4+}, W^{6+}; X = O^{2-}, F^-, OH^-), possess the cubic pyrochlore-type structure. Using an anion-centered polyhedral description, the structure of pyrochlore can be described as an anion-deficient fluorite derivative (Subramanian et al. 1984). The A and B cations form a face-centered cubic array with the anions occupying 7/8 of the tetrahedral interstices. A relative ordering of the A cations and vacancies, or the accommodation of different cations with different coordination requirements can induce a reduction in symmetry below that of the conventional ideal pyrochlore structure. The zirconolite-minerals, ideally $CaZrTi_2O_7$, and related synthetic phases exhibit polytypic relationships with the pyrochlore structure. They are based on different stacking sequences of the A_3B- and B_3A-pyrochlore-type layers, named *M* and *N*, respectively, following the notation used by Mazzi and Munno (1983). Zirconolite-3*T* is the three-layered trigonal polytypoid of $CaZrTi_2O_7$ (Mazzi and Munno 1983), the others being zirconolite-3*O* (Mazzi and Munno 1983) and zirconolite-2*M* (Gatehouse et al. 1981). Two additional polytypes, zirconolite-4*M* and -6*T* have been synthesized (Smith and Lumpkin 1993; Coelho et al. 1997). In terms of an anion-centered polyhedral description, the zirconolite-polytypes preserve the anion ordering on 7/8 of the tetrahedral interstices as observed in pyrochlore.

Both weberite-type and zirconolite-type $A_2B_2X_7$ compounds can be described as a sequence of *M* and *N* pyrochlore-type layers (see Bonazzi and Bindi 2007, their Figures 1 and 2). A and B cations form a distorted face-centered cubic array. However, the anion distribution among the interstitial cavities of the A_2B_2 array observed in pyrochlore and in the zirconolite-type compounds is not maintained in weberite-type compounds, where one of the anions moves from a tetrahedral interstice to an adjacent octahe-

* E-mail: zanazzi@unipg.it

TABLE 1. Details of data collections and structural refinements in air and in DAC at different pressures

P (GPa)	0.0001	2.25	4.23	5.41	6.38	7.42
theta-range (°)	1–28.56	1–28.34	1–28.13	1–23.09	1–28.60	1–28.05
Range of *hkl*	$-8 < h < 9$	$-9 < h < 9$	$-9 < h < 9$	$-7 < h < 7$	$-9 < h < 9$	$-9 < h < 9$
	$-9 < k < 5$	$-9 < k < 9$	$-9 < k < 9$	$-6 < k < 6$	$-9 < k < 9$	$-9 < k < 9$
	$-23 < l < 23$	$-6 < l < 6$	$-6 < l < 6$	$-6 < l < 6$	$-7 < l < 6$	$-7 < l < 6$
Refined parameters	103	45	45	45	45	45
Collected reflections	4365	5214	3312	2334	4930	3063
Independent refl.	1289	444	273	161	435	283
Refl. with $F_o > 4\sigma(F_o)$	1030	329	210	210	329	190
R_{int} (%)	3.82	11.23	10.74	8.81	8.20	8.47
R_{obs} (%)	4.55	5.80	5.46	5.04	5.49	5.82
R_{all} (%)	6.62	7.14	6.67	6.81	7.28	8.61
$\Delta\rho_{max}$ (e/Å^3)	1.09	1.32	1.63	0.75	1.26	0.98
$\Delta\rho_{min}$ (e/Å^3)	−1.48	−1.10	−1.26	−0.93	−1.27	−0.87

dral interstice. This arrangement, as well illustrated by Grey et al. (2003), is a common feature of all weberite-type polytypes.

The driving forces controlling a given compound to crystallize in one of these two competing structural types (i.e., weberite- or zirconolite-type) are still unknown; among the known $M_2^{2+}Sb_2O_7$ oxides, ingersonite (M^{2+} = ¾Ca + ¼Mn) and $Mn_2^{2+}Sb_2O_7$ (Scott 1990) crystallize with the weberite-3*T* structure, whereas $Ca_2Sb_2O_7$ occurs in both pyrochlore and weberite-2*O* structure types (Brisse et al. 1972; Knop et al. 1980) depending on the pressure applied during the synthesis, with high pressure favoring the cubic pyrochlore structure. On the other hand, $Pb_2Sb_2O_7$ has the pyrochlore structure at room temperature and transforms to the weberite structure above 510 K (Ivanov and Zavodnik 1990). The available evidence, therefore, seems to indicate that high pressures induce the conversion from a weberite-type structure to a cubic pyrochlore. It should be noted that an ideal $Fd\bar{3}m$ pyrochlore structure has a unique position (Wyckoff 16*d*) for the A cations. This feature makes ingersonite a special case of study; in fact, in the case of this mineral, Mn and Ca are ordered on independent sites; the conversion to the cubic pyrochlore structure, on the contrary, would imply a disordered distribution of Mn and Ca on the same site, which is highly unlikely at room temperature. On the other hand, the zirconolite-type structure is based on a pyrochlore-like anion distribution but allows different A and A′ cations to be ordered on independent sites. To investigate the effect of pressure on ingersonite, a crystal from the type material was studied by means of in situ single-crystal X-ray diffraction.

EXPERIMENTAL METHODS

A crystal fragment (70 × 80 × 84 μm) of natural ingersonite from the Långban mine, Värmland, Sweden (sample 163012, Smithsonian Institution, Washington, D.C.) was selected for the high-pressure X-ray diffraction experiments.

Room-pressure experiment

For the refinement at room conditions, the ingersonite crystal was mounted on an Oxford Diffraction Xcalibur3 diffractometer equipped with both CCD area and point detectors, operating at 50 kV and 35 mA, and using graphite monochromatized Mo radiation ($\lambda K\alpha_1$ = 0.7093 Å). Diffraction data were first collected with the area detector with the crystal in air. To maximize the reciprocal space coverage, a combination of ω and φ scans was used, with a step size of 0.8° and a time of 50 s/frame, for a total of 3500 frames. Data were corrected for absorption with the program SADABS (Sheldrick 1996). Details of data collection and refinement of the investigated sample are reported in Table 1.

The lattice parameters were accurately measured using the point detector and calculated by the least-squares fit of Bragg angles for about 40 selected reflections in the θ range 5–25° (Table 2). The crystal structure refinement was carried out in space group $P3_121$ with anisotropic displacement parameters, using the SHELX-97 program (Sheldrick 1997), starting from the atomic coordinates of Bonazzi and Bindi (2007). Ionized atomic scattering factors and $\Delta f'$, $\Delta f''$ coefficients from the *International Tables for X-ray Crystallography* (Wilson and Prince 1999) were used. Full occupancy was assumed for all cation sites. Site-scattering values were refined as follows: Ca^{2+} vs. Mn^{2+} (A1 and A3), Mn^{2+} vs. Sb^{5+} (A2), Sb^{5+} vs. Mg^{2+} (B1, B2, and B3); the obtained site populations together with the atomic coordinates and anisotropic displacement parameters are listed in Table 3. Table 4[1] lists the observed and calculated structure factors.

TABLE 2. Unit-cell parameters measured at different pressures

P (GPa)	*a* (Å)	*c* (Å)	*V* (Å^3)
0.0001*	7.279(3)	17.667(6)	810.7(5)
0.31	7.279(4)	17.613(21)	808(1)
1.10	7.265(7)	17.582(31)	804(1)
2.25*	7.243(3)	17.570(12)	798.3(7)
3.39	7.233(6)	17.550(38)	795(2)
4.23*	7.218(4)	17.510(11)	790.0(8)
5.04	7.209(13)	17.470(57)	786(3)
5.41*	7.204(4)	17.450(52)	784(2)
6.38*	7.182(6)	17.465(22)	780(1)
7.42*	7.170(7)	17.406(20)	775(1)

* Intensity data collected at this pressure.

High-pressure experiments

The HP behavior of ingersonite was studied with data from several mountings of fragments from the same sample. Each crystal was loaded with a chip of Sm^{2+}:BaFCl and a fragment of α-quartz, in a ETH diamond-anvil cell (DAC), equipped with type-I diamonds with 600 μm culet face diameter. The pressure chamber was a 300 μm diameter hole, drilled in a 250 μm thick steel Inconel 750X gasket preindented to 180 μm. A methanol-ethanol mixture (4:1) was used as hydrostatic pressure-transmitting medium. The wavelength shift of the 6876 Å Sm^{2+} fluorescence line was measured for an approximate estimate of the pressure (Comodi and Zanazzi 1993); the quartz crystal was used for precise measurement of the pressure (Angel et al. 1997). The uncertainties in the pressure calibration based on the equation of state of quartz were estimated to be less than 0.05 GPa. The experiments were carried out in the pressure range 10^{-4}–7.42 GPa.

The DAC was centered on the diffractometer following the procedure of Budzianowski and Katrusiak (2004). Intensity data were collected with the CCD detector, and then the lattice parameters of ingersonite and quartz were accurately measured with the point detector. Several reflections (between 20 and 40) in the θ range 5–28° were used. Results are listed in Table 2.

The intensity data were corrected for the cell and crystal absorption using the Absorb V6.1 software (Angel 2004). The least-squares refinements with data measured at 2.25, 4.23, 5.41, 6.38, and 7.42 GPa, were performed with the SHELX-97 program (Sheldrick 1997). Isotropic atomic displacement parameters were used

[1] Deposit item AM-09-010, Table 4 (observed and calculated structure factors). Deposit items are available two ways: For a paper copy contact the Business Office of the Mineralogical Society of America (see inside front cover of recent issue) for price information. For an electronic copy visit the MSA web site at http://www.minsocam.org, go to the American Mineralogist Contents, find the table of contents for the specific volume/issue wanted, and then click on the deposit link there.

for all atoms and the site occupancies were fixed to the values resulting from the refinement in air. Details of data collection and refinement are listed in Table 1. The observed and calculated structure factors are reported in Table 4[1]; fractional atomic coordinates and the displacement parameters are reported in Table 5.

Electron microprobe analysis

The crystal used for the structural study was embedded in resin and polished for the chemical analysis that was performed using a CAMECA-CAMEBAX electron microprobe operating with a fine-focused beam (~1 μm) at an acceleration voltage of 15 kV and a beam current of 15 nA. The following counting times were used: 10 s (peak) and 5 s (total background) for Ca, Mn, Mg, Fe, and Sb, and 20 s (peak) and 10 s (total background) for F. X-ray counts were converted in oxide wt% using the PAP correction program supplied by CAMECA (Pouchou and Pichoir 1985). For the WDS analyses the following lines were used: Ca$K\alpha$, Mn$K\alpha$, Mg$K\alpha$, Fe$K\alpha$, Sb$L\alpha$, and F$K\alpha$. The standards employed were wollastonite (Ca), synthetic $MnTiO_3$ (Mn), forsterite (Mg), synthetic Fe_2O_3 (Fe), synthetic Sb_2S_3 (Sb), and apatite-(CaF) (F). The crystal was found to be homogeneous within the analytical uncertainties. Average of the results of eight microprobe spots (Table 6) gave rise to the formula $(Ca_{2.77}Mn^{2+}_{1.08}Mg_{0.03}Fe^{2+}_{0.02}Sb^{5+}_{4.04})O_{14}$ on the basis of 14 O atoms. The resulting sum of electrons (289.4) is in good agreement with the value obtained by the refinement of the cation-site occupancy (287.4).

Results and discussion

Compressibility

The unit-cell parameters at various pressures are listed in Table 2 and shown in Figures 1, 2, and 3. The "normalized stress" vs. the Eulerian finite strain (Jeanloz and Hazen 1991; Angel 2000, 2001) is shown in Figure 4. Owing to the P range investigated and the quality of data, a second-order Birch-Murnaghan Equation of State (EoS) is the best approximation to describe the volume evolution of ingersonite with P, as suggested by the plot of Figure 3. The refined EoS parameters are V_0 = 810.6(1) Å^3, very close to the measured value (Table 2), and K_0 = 154.5(2.4) GPa with K' fixed to 4 (Fig. 2). Weighted χ^2 is 9, maximum ΔP is –0.3 GPa.

We determined axial compressibility by fitting axial compressions (x_{i0}/x_i) to the equation: $\beta_{xi} \cong -1/P\cdot[(x_{i0}/x_i) - 1]$ (where x_i is the selected crystallographic axis, P is pressure, and subscript 0 is ambient pressure) and assuming that β_{xi} are constant in the pressure range of interest (Fig. 3). The data fits between 10^{-4} and 7.42 GPa yielded β_a= 2.01(3) and β_c= 1.96(10) 10^{-3} GPa^{-1}, with relative compressions $c < a$ in the ratio 0.98:1. Therefore the ingersonite behavior with pressure is almost isotropic.

To date, no compressibility data of fluorides and oxides with the weberite-3T or zirconolite-3T structure have been reported in literature. We can compare the value of the bulk modulus found in ingersonite with some data determined with X-ray powder diffraction for various pyrochlore minerals with different compositions. The values of K_0 for pyrochlores measured thus far are higher than that of ingersonite, in the range 164.8(1.5) GPa ($Sm_2Ti_2O_7$; Zhang et al. 2005) to 210(4) GPa (Tb_2SnTiO_7; Kumar et al. 2006). Intermediate values are observed for $Gd_2Zr_2O_7$ [186(12) GPa; Zhang et al. 2007], $Tl_2Mn_2O_7$ [198(8)

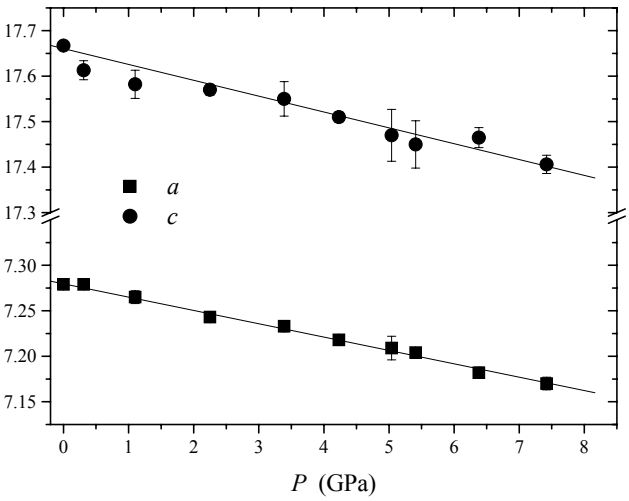

Figure 1. Lattice parameters (Å) of ingersonite as a function of pressure.

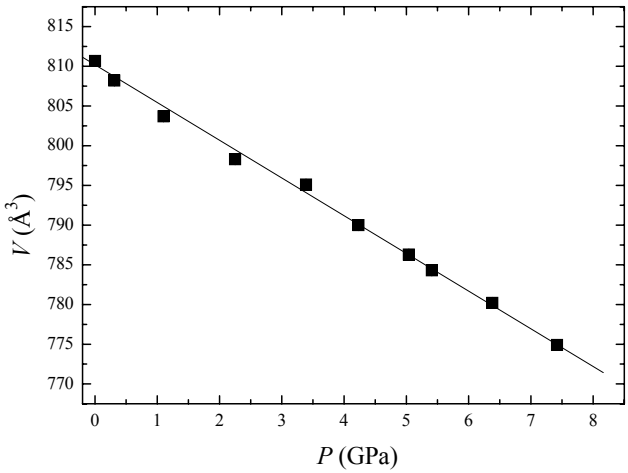

Figure 2. Variation of cell volume of ingersonite as a function of pressure. The solid line represents the second-order Birch-Murnaghan EoS best fit. The e.s.d. values are smaller than the size of the symbols.

Table 3. Atomic parameters for ingersonite in air at room conditions

	Occupancy		x/a	y/b	z/c	U_{eq}	U_{11}	U_{22}	U_{33}	U_{12}	U_{13}	U_{23}
B1	1.00Sb	3*a*	0.3205(3)	0	0.3333	0.0090(3)	0.0113(6)	0.0082(6)	0.0063(4)	0.0041(3)	0.0002(3)	0.0003(6)
B2	0.96Sb + 0.04Mg	3*b*	0.3306(3)	0	0.8333	0.0101(3)	0.0106(5)	0.0106(7)	0.0091(4)	0.0053(4)	–0.0001(3)	–0.0001(6)
B3	0.96Sb + 0.04Mg	6*c*	0.3340(3)	0.5031(5)	0.8348(1)	0.0071(2)	0.0083(5)	0.0074(4)	0.0064(3)	0.0045(5)	0.0007(3)	0.0003(3)
A1	0.92Ca + 0.08Mn	3*a*	0	0.843(2)	0.6667	0.014(1)	0.006(2)	0.019(2)	0.013(2)	0.0028(9)	–0.001(2)	–0.0004(8)
A2	0.92Mn + 0.08Sb	3*b*	0.839(1)	0	0.8333	0.0193(9)	0.024(2)	0.028(2)	0.008(1)	0.0142(9)	0.0037(7)	0.008(1)
A3	0.94Ca + 0.06Mn	6*c*	0.498(2)	0.3492(8)	0.6615(1)	0.0132(8)	0.010(1)	0.012(2)	0.013(1)	0.003(2)	–0.002(1)	0.001(1)
O1		6*c*	0.203(1)	0.217(1)	0.1469(5)	0.024(2)	0.018(5)	0.040(6)	0.020(5)	0.019(5)	0.003(4)	0.004(4)
O2		6*c*	0.549(1)	0.609(2)	0.2028(4)	0.029(2)	0.060(6)	0.040(6)	0.009(4)	0.040(6)	0.003(4)	0.002(4)
O3		6*c*	0.194(1)	0.638(1)	0.1482(4)	0.018(2)	0.003(4)	0.021(5)	0.018(4)	–0.004(3)	–0.002(4)	0.001(4)
O4		6*c*	–0.037(1)	0.310(1)	0.0561(4)	0.020(2)	0.023(5)	0.023(5)	0.018(4)	0.014(4)	–0.004(3)	–0.007(4)
O5		6*c*	–0.056(1)	0.801(2)	0.0564(4)	0.015(2)	0.016(4)	0.020(6)	0.018(4)	–0.004(3)	–0.002(4)	0.002(4)
O6		6*c*	0.539(2)	0.402(1)	0.0557(4)	0.017(2)	0.014(5)	0.021(4)	0.012(5)	0.005(5)	–0.005(5)	0.002(3)
O7		6*c*	0.540(2)	0.803(2)	0.0595(4)	0.015(2)	0.023(6)	0.012(5)	0.015(4)	0.013(3)	0.003(5)	0.002(5)

TABLE 5. Refined atomic parameters for ingersonite at different pressures

P (GPa)	2.25	4.23	5.41	6.38	7.42
			B1		
x	0.3193(4)	0.3185(5)	0.3170(7)	0.3188(5)	0.3191(8)
U_{iso}	0.012(8)	0.016(1)	0.018(1)	0.004(8)	0.015(1)
			B2		
x	0.3298(4)	0.3271(6)	0.3279(5)	0.3303(6)	0.3313(9)
U_{iso}	0.010(7)	0.013(1)	0.0142(9)	0.0085(7)	0.016(1)
			B3		
x	0.3351(4)	0.3362(6)	0.3368(5)	0.3360(3)	0.3364(8)
y	0.5002(8)	0.5035(7)	0.5006(5)	0.5001(8)	0.4986(7)
z	0.8354(3)	0.8351(4)	0.8360(3)	0.8343(3)	0.8340(4)
U_{iso}	0.0079(6)	0.014(1)	0.0132(7)	0.0033(6)	0.0114(8)
			A1		
y	0.842(2)	0.839(2)	0.832(1)	0.840(2)	0.844(3)
U_{iso}	0.013(2)	0.014(4)	0.007(2)	0.018(3)	0.018(4)
			A2		
x	0.829(2)	0.834(2)	0.829(1)	0.826(2)	0.827(3)
U_{iso}	0.024(2)	0.030(3)	0.019(3)	0.025(3)	0.026(3)
			A3		
x	0.496(2)	0.487(2)	0.487(1)	0.491(2)	0.500(3)
y	0.3457(9)	0.342(2)	0.344(1)	0.348(1)	0.349(2)
z	0.6619(7)	0.662(1)	0.6652(9)	0.6623(8)	0.659(1)
U_{iso}	0.014(2)	0.023(4)	0.010(2)	0.015(3)	0.025(3)
			O1		
x	0.198(2)	0.199(3)	0.201(3)	0.197(3)	0.199(5)
y	0.210(3)	0.220(3)	0.212(3)	0.202(4)	0.203(5)
z	0.144(3)	0.151(3)	0.151(3)	0.153(3)	0.145(3)
U_{iso}	0.031(6)	0.027(7)	0.012(6)	0.037(8)	0.023(8)
			O2		
x	0.561(2)	0.553(3)	0.565(3)	0.559(3)	0.545(5)
y	0.609(2)	0.604(3)	0.605(3)	0.609(3)	0.605(6)
z	0.199(2)	0.197(3)	0.193(5)	0.188(3)	0.172(5)
U_{iso}	0.017(4)	0.019(6)	0.034(8)	0.026(5)	0.05(1)
			O3		
x	0.194(3)	0.191(4)	0.188(3)	0.191(3)	0.197(6)
y	0.636(3)	0.634(4)	0.628(4)	0.628(3)	0.637(7)
z	0.1609(3)	0.164(4)	0.161(3)	0.154(3)	0.151(6)
U_{iso}	0.037(6)	0.06(1)	0.027(8)	0.022(7)	0.07(2)
			O4		
x	−0.028(2)	−0.030(3)	−0.024(4)	−0.035(3)	−0.046(4)
y	0.313(2)	0.317(3)	0.322(5)	0.304(3)	0.293(5)
z	0.056(3)	0.053(3)	0.048(4)	0.047(3)	0.045(4)
U_{iso}	0.024(4)	0.026(7)	0.037(8)	0.021(5)	0.029(9)
			O5		
x	−0.056(3)	−0.048(3)	−0.044(4)	−0.052(3)	−0.044(4)
y	0.798(5)	0.797(4)	0.811(6)	0.802(4)	0.799(5)
z	0.069(3)	0.065(4)	0.062(3)	0.068(3)	0.054(4)
U_{iso}	0.036(6)	0.033(8)	0.030(8)	0.018(6)	0.017(7)
			O6		
x	0.533(4)	0.527(4)	0.540(4)	0.536(4)	0.534(5)
y	0.399(2)	0.401(3)	0.399(3)	0.400(3)	0.406(3)
z	0.049(2)	0.053(3)	0.041(4)	0.042(3)	0.042(4)
U_{iso}	0.008(3)	0.008(6)	0.005(4)	0.017(5)	0.011(6)
			O7		
x	0.542(4)	0.553(4)	0.537(5)	0.552(4)	0.559(5)
y	0.815(4)	0.825(4)	0.801(6)	0.816(4)	0.819(5)
z	0.070(3)	0.065(4)	0.068(4)	0.068(3)	0.074(5)
U_{iso}	0.021(5)	0.018(7)	0.031(7)	0.017(6)	0.031(9)

GPa; Velasco et al. 2003], and $Gd_2Ti_2O_7$ [208(8) GPa; Saha et al. 2006]. Since all these compounds are cubic or pseudocubic, the dispersion of these values should be ascribed to the different compositions rather than to a different structural arrangement.

TABLE 6. Electron microprobe data for the selected ingersonite crystal

	wt% *	Range	Atomic ratios
CaO	17.28	17.14–17.45	2.77
MnO	8.55	8.32–8.77	1.08
MgO	0.15	0.11–0.22	0.03
FeO	0.14	0.07–0.20	0.02
Sb_2O_5	72.82	71.57–73.74	4.04
Total	98.94	97.79–99.98	

Notes: Chemical formula was calculated on the basis of 14 O atoms.
* Average of eight spot analyses.

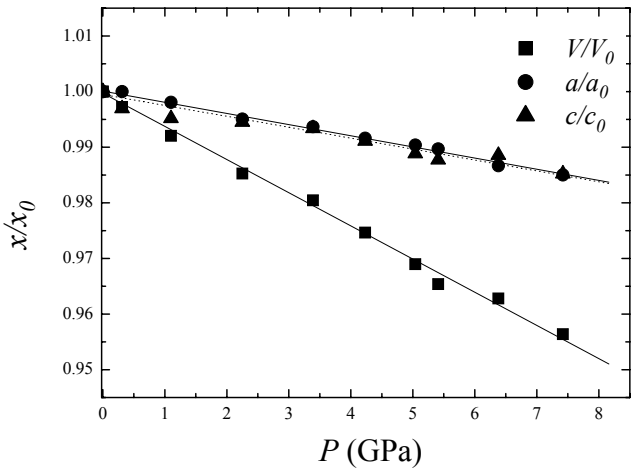

FIGURE 3. Variation of the unit-cell parameters as a function of *P* for ingersonite, normalized with respect to the room-pressure value. The e.s.d. values are smaller than the size of the symbols.

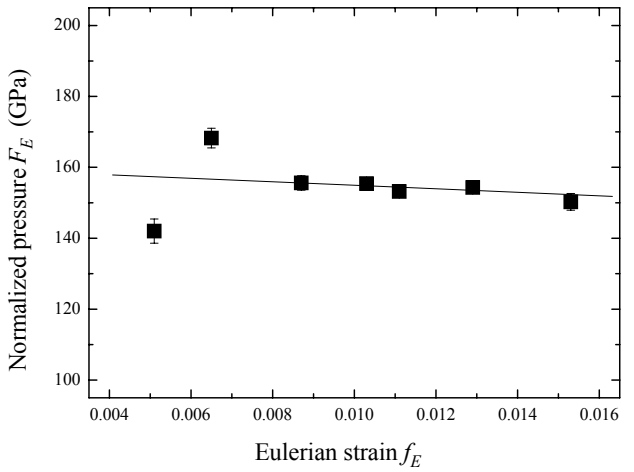

FIGURE 4. Plot of "normalized stress" defined as $F_E = P/[3f_E(1 + 2f_E)^{5/2}]$, vs. finite strain $f_E = [(V_0/V)^{2/3} - 1]/2$. The first two points were omitted.

Structural evolution with *P*

The structure of ingersonite can be described as a sequence of pairs of polyhedral layers (*M* and *N*) stacked along [001]. As far as the cation sites are concerned, *M* and *N* layers have general formulae AB_3 and A_3B, respectively, where B are the octahedrally coordinated cations (B1, B2, and B3) that accommodate Sb^{5+} with very minor substitution by lighter divalent cations or minor vacancies (Table 3). The octahedral framework gives rise to three types of larger cavities, which host Ca (A1

and A3) and Mn^{2+} (A2).

Variations in bond distances and polyhedral volumes with *P* are listed in Table 7. Due to the high errors affecting structural data relative to the range of variations, no fitting was possible to describe significantly the evolution of the polyhedral volumes with *P*. Nonetheless, some considerations can be made. The overall mean <B-O> distance is quite constant, indicating almost no compressibility of the Sb^{5+} octahedra; this feature is in keeping with what is observed for octahedral Sb^{5+} in the structures of both α and β modifications of Sb_2O_4. In-situ high-pressure synchrotron X-ray experiments, indeed, have shown that in these compounds, the <Sb^{5+}-O> distance varies from 2.003 Å (at 0.0001 GPa) to 1.993 Å (at 9.8 GPa) and from 1.981 Å (at 0.0001 GPa) to 1.978 Å (at 9.2 GPa) in α-Sb_2O_4 and β-Sb_2O_4, respectively (Orosel et al. 2005). In the *P* range investigated the ^{VI}<A2-O> distance also exhibits only minor variations (Table 7). However, an increase in pressure induces marked variations in the pyrochlore-like *M* layer where A2 is located. In Figure 5, the pseudohexagonal arrangement of cations (i.e., B2 and B3) and anions (O1, O2, and O3) surrounding the A2 cation in the pyrochlore-like *M* layer is shown; the mean of the six independent B-O distances belonging to the layer (<d> in Fig. 6a) decreases linearly from 1.98 to 1.92 Å; due to the fact that the A2 polyhedron is rather rigid, the relative displacement of B2 and B3 toward A2 causes an increase of the <B-O-B> angle (<δ> in Fig. 6b). The variation of these

TABLE 7. Selected bond lengths (Å) and volumes (Å^3) from structure refinements

P (GPa)	0.0001	2.25	4.23	5.41	6.38	7.42
B1-O7(×2)	1.964(7)	2.11(4)	2.05(4)	2.03(5)	2.03(4)	2.07(7)
O5(×2)	1.944(7)	2.05(3)	2.04(4)	2.02(4)	2.04(3)	1.95(3)
O6(×2)	2.007(7)	1.96(2)	1.99(3)	1.91(3)	1.90(3)	1.86(3)
<B1-O>	1.972	2.04	2.03	1.99	1.99	1.96
V(B1)	10.02(5)	11.2(1)	10.9(1)	10.1(1)	10.2(1)	9.7(1)
B2-O3(×2)	1.987(9)	1.95(2)	1.94(3)	1.89(2)	1.89(2)	1.94(5)
O5(×2)	1.968(7)	1.95(4)	2.00(6)	2.08(7)	2.10(5)	2.14(7)
O1(×2)	2.052(9)	2.05(2)	1.96(2)	2.02(2)	2.05(3)	2.08(4)
<B2-O>	2.002	1.98	1.97	2.00	2.01	2.06
V(B2)	10.42(5)	10.1(1)	9.9(1)	10.3(1)	10.6(1)	11.2(1)
B3-O1	1.934(9)	1.94(2)	1.94(2)	1.89(2)	1.90(2)	1.90(3)
O2	1.934(9)	1.90(2)	1.87(3)	1.82(3)	1.83(2)	1.79(4)
O2	1.973(9)	1.97(2)	1.95(2)	1.99(3)	1.91(2)	1.85(4)
O3	1.965(9)	1.95(2)	1.94(3)	1.98(2)	1.97(2)	1.94(4)
O7	1.972(7)	1.78(5)	1.87(6)	1.83(7)	1.80(6)	1.70(9)
O6	1.982(7)	2.07(4)	2.00(6)	2.18(6)	2.20(6)	2.20(7)
<B3-O>	1.960	1.94	1.93	1.95	1.94	1.90
V(B3)	9.90(5)	9.5(1)	9.5(1)	9.8(1)	9.6(1)	8.9(1)
A1-O5(×2)	2.47(2)	2.57(4)	2.55(4)	2.49(4)	2.53(3)	2.41(4)
O4(×2)	2.406(8)	2.36(2)	2.36(3)	2.32(3)	2.27(2)	2.26(3)
O6(×2)	2.63(2)	2.53(3)	2.50(3)	2.45(3)	2.48(3)	2.50(4)
O1(×2)	2.626(8)	2.55(4)	2.67(6)	2.65(4)	2.69(5)	2.54(6)
<A1-O>	2.53	2.50	2.52	2.48	2.49	2.43
V(A1)	25.06(5)	24.4(1)	24.8(1)	24.3(1)	24.6(1)	22.6(1)
A2-O5(×2)	1.981(7)	1.75(5)	1.81(7)	1.85(6)	1.75(5)	1.99(6)
O1(×2)	2.41(1)	2.42(2)	2.44(2)	2.41(2)	2.35(3)	2.37(4)
O3(×2)	2.51(1)	2.42(2)	2.44(3)	2.43(2)	2.43(2)	2.42(4)
O2(×2)	2.91(2)	2.81(3)	2.84(3)	2.75(2)	2.77(2)	2.83(4)
^{VI}<A2-O>	2.30	2.20	2.24	2.22	2.18	2.25
^{VIII}<A2-O>	2.45	2.35	2.38	2.36	2.33	2.40
^{VI}V(A2)	14.26(5)	12.2(1)	12.6(1)	12.5(1)	11.7(1)	13.5(1)
^{VIII}V(A2)	23.2(5)	19.7(1)	20.6(1)	20.4(1)	19.1(1)	21.8(1)
A3-O4	2.246(8)	2.26(3)	2.20(3)	2.18(4)	2.14(3)	2.09(4)
O4	2.33(1)	2.32(2)	2.29(3)	2.24(4)	2.29(3)	2.32(4)
O5	2.42(1)	2.48(4)	2.34(4)	2.38(5)	2.42(4)	2.28(5)
O7	2.50(1)	2.51(4)	2.38(4)	2.48(4)	2.44(4)	2.56(6)
O6	2.59(1)	2.55(3)	2.66(4)	2.49(3)	2.51(3)	2.52(4)
O7	2.67(1)	2.72(4)	2.77(4)	2.74(5)	2.79(3)	2.80(5)
O2	2.709(8)	2.79(4)	2.80(6)	2.83(8)	2.93(5)	3.20(5)
O3	2.556(7)	2.77(5)	2.83(7)	2.82(6)	2.65(5)	2.50(1)
^{VIII}<A3-O>	2.51	2.55	2.53	2.52	–	–
^{VII}<A3-O>	–	–	–	–	2.46	2.44
^{VIII}V(A3)	25.18(5)	26.5(1)	25.9(1)	25.1(1)	–	–
^{VII}V(A3)	–	–	–	–	20.2(1)	19.6(1)
V(O1)	5.55(5)	5.5(1)	5.4(1)	5.4(1)	5.5(1)	5.4(1)
**V*(O2)	22.55(5)	22.2(1)	22.0(1)	21.8(1)	21.7(1)	21.6(1)
V(O3)	5.53(5)	5.4(1)	5.4(1)	5.4(1)	5.2(1)	5.1(1)
V(O4)	5.62(5)	5.5(1)	5.5(1)	5.5(1)	5.4(1)	5.4(1)
V(O5)	5.30(5)	5.2(1)	5.1(1)	5.1(1)	5.1(1)	5.0(1)
V(O6)	5.92(5)	5.9(1)	5.9(1)	5.7(1)	5.8(1)	5.7(1)
V(O7)	5.68(5)	5.6(1)	5.5(1)	5.5(1)	5.4(1)	5.4(1)

* Volume of the octahedral cavity.

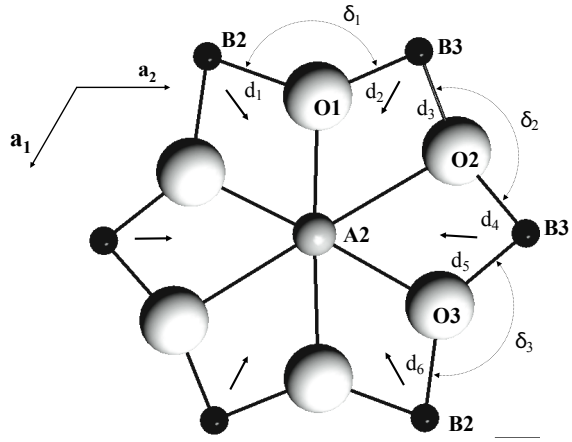

FIGURE 5. Pseudohexagonal arrangement of B cations and anions surrounding the A2 cation in the pyrochlore-like AB_3 layer.

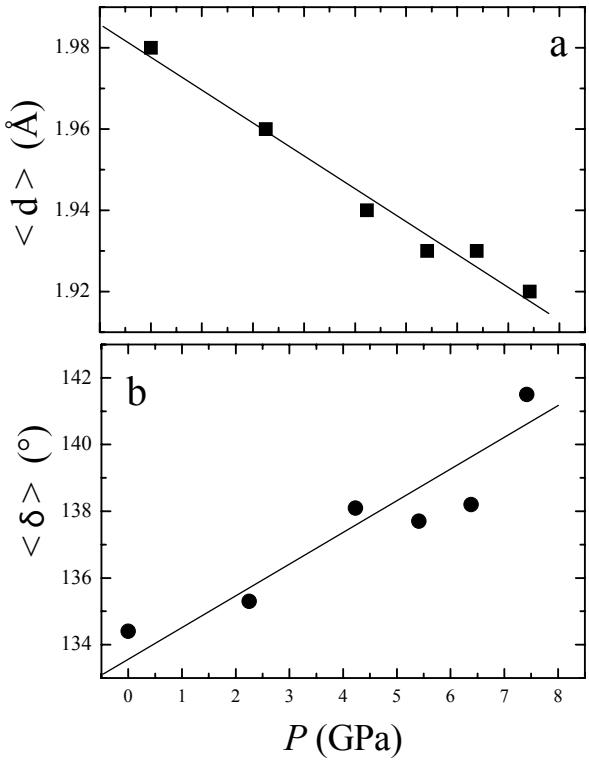

FIGURE 6. Variation of <d> and <δ> as a function of pressure. [<d> = $(d_1 + d_2 + d_3 + d_4 + d_5 + d_6)/6$ and <δ> = $(\delta_1 + \delta_2 + \delta_3)/3$ as in Fig. 5.]

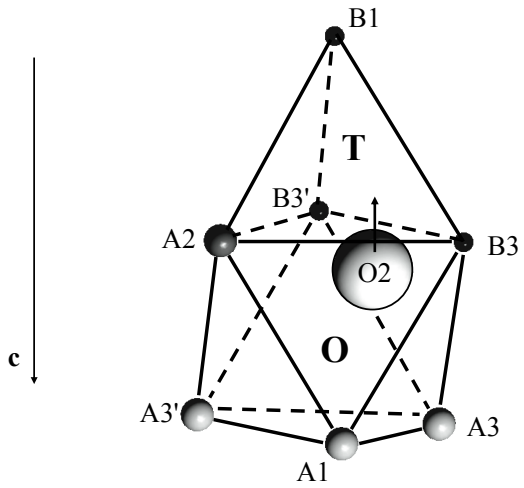

FIGURE 7. Structural sketch showing the migration of the O2 atom from the A_4B_2 octahedral cavity (O) toward the adjacent AB_3 tetrahedral cavity (T). See text for explanation.

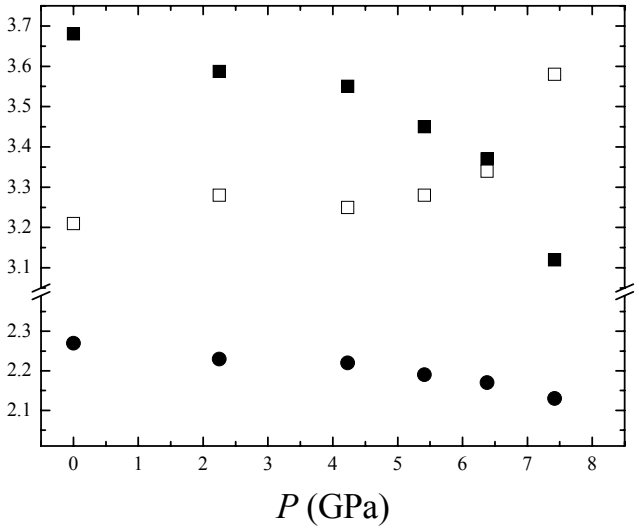

FIGURE 8. Change of the O2 atom environment as a function of *P* (see Fig. 7). Empty squares represent the average of the three O2-A1, -A3, -A3′ distances (Å); filled circles represent the average of the three O2-A2, -B3, -B3′ distances (Å); and filled squares represent O2-B1 distance (Å).

parameters as a function of pressure was also examined in the cubic structure of the $(Tl_{2-x}A_x)(Mn_{2-x}B_x)O_7$ (A = Bi, Cd; B = Sb) pyroclore-like compounds (Velasco et al. 2003). These authors have shown that the B-O distance decreases independently from substitutions at the A and B sites, whereas the B-O-B angle shows different variations as a function of the relative A-O and B-O bonding strengths. In particular, when A-O bonds are less compressible than B-O bonds, both B-O and B-O-B decrease with pressure, whereas they vary in the opposite way when A-O bonds are more compressible than B-O bonds. In this view, it would appear that Sb-O bonds, at least within the *M* layer, are more compressible than the Mn^{2+} bonds.

The largest structural change is observed for the *z* coordinate of the O2 atom. As a first consequence of the shift of this atom, a dramatic lengthening of the A3-O2 distance is observed (from 2.710 to 3.20 Å), so that from 6.38 GPa the A3 cation is properly described as sevenfold coordinated. Using an anion-centered polyhedral description, O2 is the only O atom that is asymmetrically located in an octahedral interstice, this feature being the most remarkable difference between the structure of ingersonite (i.e., weberite-3*T* type, space group $P3_121$) and that of zirconolite-3*T* (space group $P3_121$), where all the O atoms occupy the tetrahedral interstices of a cubic A_2B_2 array. As shown in Figure 7, the O2 atom migrates from the A_4B_2 octahedral cavity toward the adjacent AB_3 tetrahedral cavity. As the pressure increases, O2 moves away from the A1-A3-A3′ octahedral face (empty squares in Fig. 8 represent the average of the three O2-A1, -A3, -A3′ distances) and approaches the A2-B3-B3′ face (filled circles in Fig. 8 represent the average of the three O2-A2, -B3, -B3′ distances). Indeed, at 7.42 GPa the O2 is close to the face shared between tetrahedral and octahedral cavity, although is still too far to link to the apical B1 cation (filled squares in Fig. 8). In principle, if a transition from weberite-3*T* to zirconolite-3*T* structure type actually occurs at higher pressures, it would imply that O2 adopts a planar triangular coordination (Φ = A2-O2-B3 + B3′-O2-B3 + B3′-O2-A2 = 360°). The plot of Φ as a function of *P* (Fig. 9) lets us speculate that this structural configuration

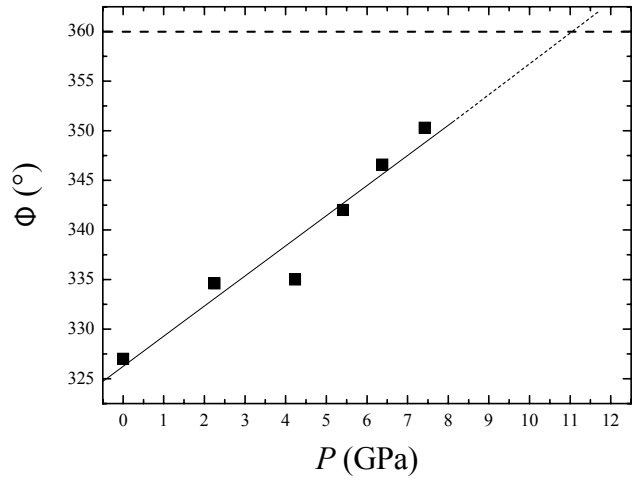

FIGURE 9. Variation of Φ as a function of *P* (Φ = A2-O2-B3 + B3′-O2-B3 + B3′-O2-A2) showing that the O2 atom could adopt a planar triangular coordination at 11 GPa, approximately.

occurs at a pressure higher than 11 GPa, approximately. Further experimental work at higher pressure is required to confirm this hypothesis.

ACKNOWLEDGMENTS

The authors thank Kimberly Tait, an anonymous referee, and the Associate Editor Przemyslaw Dera for careful reading of the text and constructive comments. This work was funded by M.I.U.R., P.R.I.N. 2006 project "Studi sperimentali su materiali geologici alle alte pressioni e temperature."

REFERENCES CITED

Angel, R.J. (2000) Equation of state. In R.M. Hazen and R.T. Downs, Eds., High-Temperature and High-Pressure Crystal Chemistry, 41, p. 35–59. Reviews in Mineralogy and Geochemistry, Mineralogical Society of America, Chantilly, Virginia.

——— (2001) EOS-FIT V6.0. Computer program. Crystallography Laboratory,

Department of Geological Sciences, Virginia Tech, Blacksburg, Virginia.
——— (2004) Absorption corrections for diamond-anvil cells implemented in the software package Absorb 6.0. Journal of Applied Crystallography, 37, 486–492.
Angel, R.J., Allan, D.R., Miletich, R., and Finger, L.W. (1997) The use of quartz as an internal pressure standard in high-pressure crystallography. Journal of Applied Crystallography, 30, 461–466.
Bonazzi, P. and Bindi, L. (2007) The crystal structure of ingersonite, $Ca_3Mn^{2+}Sb_4^{5+}O_{14}$, and its relationships with pyrochlore. American Mineralogist, 92, 947–953.
Brisse, F., Stewart, D.J., Seidl, V., and Knop, O. (1972) Pyrochlores. VIII. Pyrochlores and related compounds and minerals. Canadian Journal of Chemistry, 50, 3648–3666.
Budzianowski, A. and Katrusiak, A. (2004) High-pressure crystallographic experiments with a CCD-detector. In A. Katrusiak and P. McMillan, Eds., High-Pressure Crystallography, p. 101–112. Kluver Academic Publishers, The Netherlands.
Coelho, A.A., Cheary, R.W., and Smith, K.L. (1997) Analysis and structural determination of Nd-substituted zirconolite-4*M*. Journal of Solid State Chemistry, 129, 346–359.
Comodi, P. and Zanazzi, P.F. (1993) Improved calibration curve for the Sm^{2+}:BaFCl pressure sensor. Journal of Applied Crystallography, 26, 843–845.
Gatehouse, B.M., Grey, I.E., Hill, R.J., and Rossell, H.J. (1981) Zirconolite, $CaZr_xTi_{3-x}O_7$; structure refinements for near-end-member compositions with $x = 0.85$ and 1.30. Acta Crystallographica, B37, 306–312.
Giuseppetti, G. and Tadini, C. (1978) Re-examination of the crystal structure of weberite. Tschermaks Mineralogische und Petrographische Mitteilungen, 25, 57–62.
Grey, I.E. and Roth, R.S. (2000) New calcium tantalate polytypes in the system $Ca_2Ta_2O_7$-$Sm_2Ti_2O_7$. Journal of Solid State Chemistry, 150, 167–177.
Grey, I.E., Mumme, W.G., Ness, T.J., Roth, R.S., and Smith, K.L. (2003) Structural relations between weberite and zirconolite polytypes—refinements of doped 3*T* and 4*M* $Ca_2Ta_2O_7$ and 3*T* $CaZrTi_2O_7$. Journal of Solid State Chemistry, 174, 285–295.
Ivanov, S.A. and Zavodnik, V.E. (1990) Crystal structure of lead antimonate ($Pb_2Sb_2O_7$). Kristallografiya, 35, 842–846.
Jeanloz, R. and Hazen, R.M. (1991) Finite-strain analysis of relative compressibilities. Application to the high-pressure wadsleyite phase as an illustration. American Mineralogist, 76, 1765–1768.
Knop, O., Demazeau, G., and Hagenmuller, P. (1980) Pyrochlores. XI. High-pressure studies of the antimonates $A_2Sb_2O_7$ (A = Ca, Sr, Cd) and preparation of the weberite $Sr_2Bi_2O_7$. Canadian Journal of Chemistry, 58, 2221–2224.
Kumar, R.S., Cornelius, A.L., Nicol, M.F., Kam, K.C., Cheetham, A.K., and Gardner, J.S. (2006) Pressure-induced structural transitions in Tb-pyrochlore oxides. Applied Physics Letters, 88, 031903.
Mazzi, F. and Munno, R. (1983) Calciobetafite (new mineral of the pyrochlore group) and related minerals from Campi Flegrei, Italy; crystal structures of polymignyte and zirkelite: comparison with pyrochlore and zirconolite. American Mineralogist, 68, 262–276.
Orosel, D., Balog, P., Liu, H., Qian, J., and Jansen, M. (2005) Sb_2O_4 at high pressures and high temperatures. Journal of Solid State Chemistry, 178, 2602–2607.
Pouchou, J.L. and Pichoir, F. (1985) PAP phi-rho-Z procedure for improved quantitative microanalysis. In J.L. Armstrong, Ed., Microbeam Analysis, p. 104–106. San Francisco Press, Inc., California.
Saha, S., Muthu, D.V.S., Pascanut, C., Dragoe, N., Suryanarayanan, R., Dhalenne, G., Revcolevschi, A., Karmakar, S., Sharma, S.M., and Sood, A.K. (2006) High-pressure Raman and X-ray study of the spin-frustrated pyrochlore $Gd_2Ti_2O_7$. Physical Review B, 74, 064109.
Scott, H.G. (1990) Refinement of the crystal structure of the manganese antimonate $Mn_2Sb_2O_7$ with neutron powder diffraction data by the profile decomposition method. Zeitschrift für Kristallographie, 190, 41–46.
Sheldrick, G.M. (1996) SADABS. Program for empirical absorption correction of area detector data. Institut für Anorganische Chemie, University of Göttingen, Germany
——— (1997) SHELX-97. Programs for crystal structure determination and refinement. Institut für Anorganische Chemie, University of Göttingen, Germany.
Smith, K.L. and Lumpkin, G.R. (1993) Structural features of zirconolite, hollandite and perovskite, the major waste-bearing phases in Synroc. In J.N. Bolan and J.D. FitzGerald, Eds., Defects and Processes in the Solid State: Geoscience Applications, p. 401–422. The McLaren Volume, Elsevier, Amsterdam.
Subramanian, M.A., Clearfield, A., Umarji, A.M., Shenoy, G.K., and Subba Rao, G.V. (1984) Synthesis and solid state studies on $Mn_2Sb_2O_7$ and $(Mn_{1-x}Cd_x)_2Sb_2O_7$ pyrochlores. Journal of Solid State Chemistry, 52, 124–129.
Velasco, P., Alonso, J.A., Tissen, V.G., Marshall, W.G., Casais, M.T., Martinez-Lope, M.J., de Andrés, A., Prieto, C., and Martinez, J.L. (2003) Pressure effect in the structure, transport properties, and magnetic interactions of $Tl_2Mn_2O_7$ pyrochlore derivatives. Physical Review B, 67, 104403.
Wilson, A.J.C. and Prince, E. (1999) International Tables for X-ray Crystallography, Volume C: Mathematical, Physical and Chemical Tables, 2nd edition. Kluwer Academic, Dordrecht.
Yakubovich, O.V., Urusov, V.S., Massa, W., Frenzen, G., and Babel, D. (1994). Crystal-chemical relations in weberite-group minerals, $Na_2M^{II}M^{III}F_7$, as derivatives of fluorite. Geologiya, 6, 19–25 (in Russian, English abstract).
Zhang, F.X., Manoun, B., Saxena, S.K., and Zha, C.S. (2005) Structure change of pyrochlore $Sm_2Ti_2O_7$ at high pressures. Applied Physics Letters, 86, 181906.
Zhang, F.X., Lian, J., Becker, U., Ewing, R.C., Hu, J., and Saxena, S.K. (2007) High-pressure structural changes in the $Gd_2Zr_2O_7$ pyrochlore. Physical Review B, 76, 214104.

Manuscript received June 3, 2008
Manuscript accepted October 27, 2008
Manuscript handled by Przemyslaw Dera